Electrostatic turbulence driven by high magnetohydrodynamic activity in Tokamak Chauffage Alfvén Brésilien

Zwinglio O. Guimarães-Filho,[1] Iberê L. Caldas,[1] Ricardo L. Viana,[2,a)]
Maria Vittoria A. P. Heller,[1] Ivan C. Nascimento,[1] Yuri K. Kuznetsov,[1]
and Roger D. Bengtson[3]
[1]*Instituto de Física, Universidade de São Paulo, 05315-970 São Paulo, São Paulo, Brazil*
[2]*Departamento de Física, Universidade Federal do Paraná, 81531-990 Curitiba, Paraná, Brazil*
[3]*Fusion Research Center, University of Texas at Austin, Austin, Texas 78712-1068, USA*

(Received 5 December 2007; accepted 16 April 2008; published online 3 June 2008)

In Tokamak Chauffage Alfvén Brésilien [R. M. O. Galvão *et al.*, Plasma Phys. Controlled Fusion **43**, 1181 (2001)], high magnetohydrodynamic (MHD) activity may appear spontaneously or during discharges with a voltage biased electrode inserted at the plasma edge. The turbulent electrostatic fluctuations, measured by Langmuir probes, are modulated by Mirnov oscillations presenting a dominant peak with a common frequency around 10 kHz. We report the occurrence of phase locking of the turbulent potential fluctuations driven by MHD activity at this frequency. Using wavelet cross-spectral analysis, we characterized the phase and frequency synchronization in the plasma edge region. We introduced an order parameter to characterize the radial dependence of the phase-locking intensity. © *2008 American Institute of Physics*. [DOI: 10.1063/1.2920211]

I. INTRODUCTION

Many experiments have confirmed that the plasma confinement in toroidal devices depends in many ways on the fluctuating electric and magnetic fields at the plasma edge.[1–3] Magnetic fluctuations reduce plasma performance and limit relevant parameters like the poloidal beta due to the change of the plasma profiles induced by magnetic instabilities such as the tearing modes.[1] Electrostatic turbulence is the main cause of anomalous particle transport at the tokamak plasma edge that reduces the particle confinement.[2–4]

Although in some toroidal devices, as the reversed field pinches (see, for example, the experiments in Extrap T1 reversed-field pinch[5]), both electrostatic and magnetic fluctuations directly contribute to the edge transport, in tokamaks edge transport is typically determined only by electrostatic fluctuations.[2] However, Mirnov oscillations have also been found to be associated with decreased energy confinement[6] and particle confinement.[7] Furthermore, several experiments in tokamaks show that, under special conditions, the edge particle transport can be influenced by the magnetic oscillations. Thus, experiments performed with ergodic divertors in Texas Experimental Tokamak (TEXT),[8] Tore Supra,[9,10] Torus Experiment for Technology Oriented Research (TEXTOR),[11] Hybtok-II,[12] and DIII-D[13] demonstrated that an ergodized magnetic boundary can influence parameter profiles and reduce the transport. Beside this experimental evidence, some theoretical works also predict a possible influence of magnetic fluctuations on the collisional drift-wave turbulence in tokamaks.[14–16]

Experiments in the linear, magnetized, low-β plasma device Mirabelle showed spatiotemporal synchronization of drift wave turbulence.[17] This was modeled by a current profile with a prescribed mode structure and frequency. In this work, we argue that some specific experiments in tokamaks indicate that turbulence synchronization similar to this may be driven by Mirnov oscillations. Namely, in Texas Experimental Tokamak Upgrade (TEXTUp), for the first time, the edge turbulence associated with large magnetohydrodynamics (MHD) activity was systematically studied.[18] The turbulence was dramatically enhanced for the large MHD activity discharges with a 2/1 (where $m=2$ and $n=1$ are the poloidal and toroidal mode numbers, respectively) dominant mode with a measured frequency of 3 kHz. Modulations were seen in the edge density, floating potential, and electron temperature associated with the Mirnov oscillations measured by the magnetic field coils. This kind of modulation was also observed for other natural dominant magnetic modes in the Tokamak from Brazil (TBR)[19] and CASTOR,[20,21] and in Tokamak Chauffage Alfvén Brésilien (TCABR) for a 2/1 dominant magnetic mode created by an ergodic magnetic limiter.[22]

In the TCABR tokamak, plasma confinement can be improved using a voltage biased electrode inserted at the tokamak edge.[23] Investigations of MHD activity for some experimental conditions show that, after the application of the bias, the MHD activity can increase in different times and reach high amplitudes with a dominant 2/1 mode and a sideband 3/1 mode.[24] The onset of high MHD activity during these discharges produces evidence of coupling of electrostatic turbulence and magnetic fluctuation in TCABR. However, such coupling can also be observed without voltage biasing, whenever the MHD activity increases significantly.[24] Even so, we have analyzed discharges with electrode bias, since the increase in MHD activity is more likely to occur in this case.

In this paper, we report the observation of a feature of the coupling between MHD activity and electrostatic fluctua-

a)Author to whom correspondence should be addressed. Electronic mail: viana@fisica.ufpr.br.

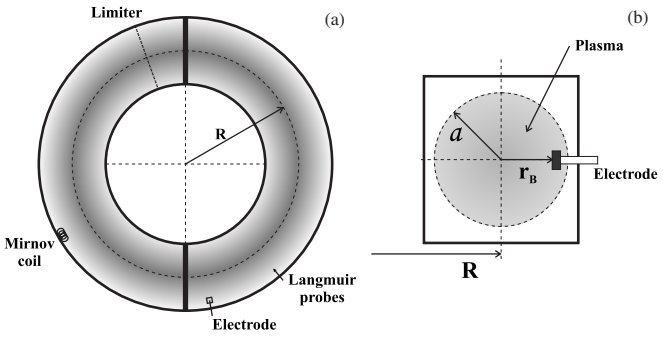

FIG. 1. Scheme of the experimental setup: (a) viewed from above; (b) cross-sectional view.

tions in the TCABR tokamak. The latter is distinguished from a simple correlation since Mirnov oscillations modulate the electrostatic potential fluctuations at the tokamak plasma edge. Different frequency peaks of the MHD activity modulate the previously uncorrelated potential fluctuations, in the sense that the latter acquire the *same* frequency peaks of the former, and they oscillate with a constant phase difference. Moreover, the usually broadband wave number and frequency spectrum characteristic of electrostatic turbulence is modified during periods of high MHD activity with a well-defined peak at $f \sim 10$ kHz and $k \sim 0$. This was revealed through wavelet spectrogram analysis (cross-spectrum) of MHD activity and turbulence fluctuations and an order parameter obtained from the phase angle between signals of floating potential and ion saturation current measured in poloidally separated electrostatic probes.

The rest of the paper is organized as follows. In the second section, we briefly describe the experiment and the kind of turbulent data we obtain from the tokamak. Section III presents the data analysis using the wavelet spectrum, as well as the corresponding order parameter. The final section contains our conclusions.

II. EXPERIMENT

The experiments were performed in a hydrogen circular plasma in the Brazilian tokamak TCABR[23,25] (major radius $R=61$ cm and minor radius $a=18$ cm). The plasma current reaches a maximum value of 100 kA with duration 100 ms. The hydrogen filling pressure is 3×10^{-4} Pa and toroidal magnetic field $B_T=1.1$ T. At the scrape-off layer the electron plasma density is $n_e \approx 1.5\times10^{18}$ m^{-3}, with an electron temperature $T_e \approx 5$ eV.

In this work, we analyze fluctuations measured at the region comprising the plasma edge and the scrape-off layer ($r \approx a$). A set of three movable electrostatic probes was used to measure the floating plasma potentials in two poloidal positions separated by 0.4 cm and the ion saturation current at a toroidal position 0.4 cm apart from the poloidal probes. With these probes we measured the ion saturation current I_s and floating potentials, φ_1 and φ_2, at the edge and scrape-off layer. The whole set was mounted at the outer equatorial region of the tokamak [Fig. 1(a)]. Radial profiles of electrostatic fluctuations were obtained on a shot-to-shot basis. Magnetic fluctuations were detected using a Mirnov coil located at $r=19.5$ cm (i.e., 1.5 cm outside the plasma radius). Probe and Mirnov coil data were digitized at 1 and 0.25 megasample per second, respectively, and filtered by a 300 kHz anti-aliasing filter. A movable electrode with a positive voltage bias of 350 V was positioned 1.5 cm inside the plasma ($r_B/a=0.92$) at the equatorial plane and low field side of the plasma column [Fig. 1(b)], 160° from the graphite limiter in the plasma current direction (counterclockwise top view).

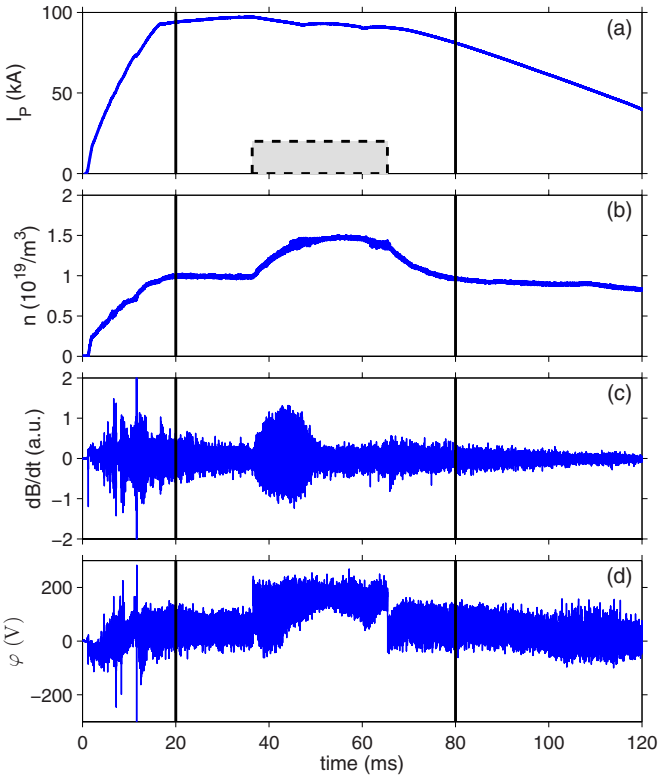

FIG. 2. (Color online) Time evolution of the (a) plasma current, (b) central estimated plasma density, (c) MHD activity, and (d) floating potential (at $r/a=0.94$) for a discharge of the TCABR tokamak with bias polarization (Shot No. 18011). The rectangular bar in (a) indicates the DC bias potential at the electrode. The vertical lines indicate the time window used in data analysis.

Figure 2 shows the time evolution of a typical tokamak plasma discharge in TCABR (Shot No. 18011). The vertical bars indicate the window chosen for analyses of the floating potential and ion saturation current fluctuations and Mirnov oscillations (to determine the MHD activity). The plasma current [Fig. 2(a)] grows rapidly in the first 20 ms and reaches a plateau where the current stays at a 100 kA level, decaying slowly during the second half until the eventual disruptions. The DC bias is switched on for 29 ms at 37 ms after the beginning of the discharge, indicated by a lower bar in Fig. 2(a). The central estimated electron density, indicated by Fig. 2(b), exhibits a similar evolution, with a first plateau level of $n_e \sim 1.0\times10^{19}$ m^{-3}, followed by an increase and a second plateau of $\sim 1.5\times10^{19}$ m^{-3} during the application of the DC bias.

The MHD activity measured by $\tilde{B}$ coils is depicted in Fig. 2(c). The magnetic fluctuations grow during the DC bias application at unpredictable times. The interesting signals are

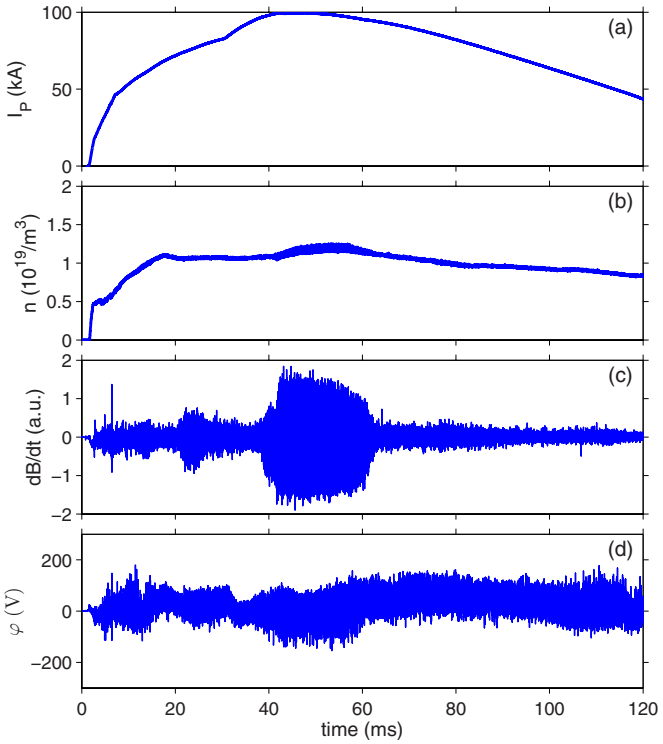

FIG. 3. (Color online) Time evolution of the (a) plasma current, (b) central estimated plasma density, (c) MHD activity, and (d) floating potential (at $r/a=0.94$) for another kind of TCABR discharge with high MHD activity without bias polarization (Shot No. 18369).

the floating electrostatic potential φ, a representative example being shown by Fig. 2(d), with highly irregular fluctuations roughly in the −100 to +100 V range (standard deviation of ~30 V). After the application of the DC bias voltage, the electrostatic fluctuations increase their standard deviation to ~65 V.

Figure 3 shows a representative example (Shot No. 18369) of another kind of discharge in TCABR in which the MHD activity increases even without biasing.[24] Thus, in this discharge we observed spontaneously strong MHD activity between 40 and 60 ms. In this case, the electrostatic fluctuations are also influenced by the magnetic activity, as in Fig. 2.

III. METHODS AND RESULTS

A. Fourier spectrum analysis

We performed Fourier spectrum analysis of the electrostatic potential fluctuations and of the MHD oscillations, as shown in Fig. 4. The tokamak discharges we analyze present periods of both weak and strong MHD activity, and the spectral properties of the signals are greatly influenced by this fact. Figure 4(a) exhibits the power spectrum for weak MHD activity (thick line) and potential fluctuations (dashed line). The magnetic oscillations have a broad spectrum, with a pronounced peak at ≈25 kHz, whereas the potential fluctuations are broadband without a peak. As the MHD activity increases, however, the Fourier power spectra of both signals nearly coincide, exhibiting a peak at the lowest Mirnov characteristic frequency of ≈10 kHz.

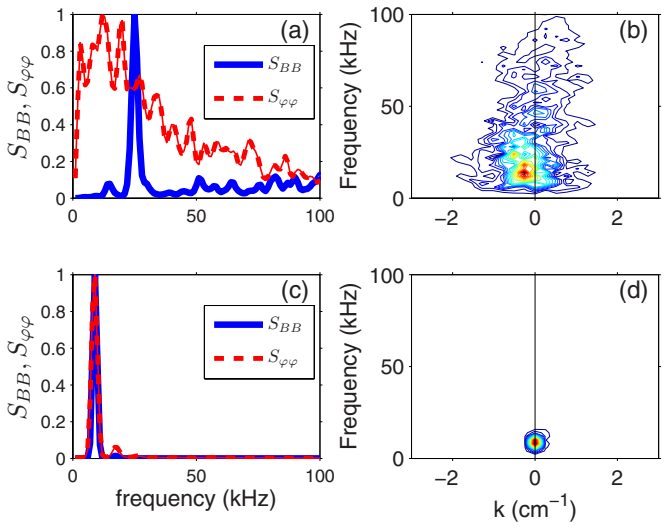

FIG. 4. (Color online) Fourier power spectral density (arbitrary units) for MHD activity (blue thick line) and fluctuating electrostatic potential (red dashed line) at $r/a=0.94$. (a) Without and (b) with strong MHD activity. Frequency and wave-number spectrum for electrostatic potential without (b) and with (d) strong MHD activity.

This near coincidence of both spectra characterizes a modulation of the electrostatic potential by magnetic oscillations, the latter driving the former since it keeps its dominant frequency and imparts it to the potential turbulent fluctuations. The influence of the MHD activity is not limited to the time domain, though, since it also produces observable effects on the spatial distribution of wave numbers. This fact is captured by the wave number and frequency spectra shown in Figs. 4(b) and 4(d), obtained without and with strong MHD activity, respectively. The spectrum of potential fluctuations is not only narrow at the Mirnov frequency but also in the wave-number domain, drifting from small negative k values to almost vanishing k. In this sense, we refer to a phase-locked electrostatic turbulence driven by high MHD activity.

This second result shows that the potential oscillations, though aperiodic in time, have the same dominant frequency of the Mirnov oscillations, and a narrow wave-number spectrum. This represents a condensation of the wave-number spectrum to a few spatial modes. If we think of the potential fluctuations as coming from a chain of coupled identical oscillators, it turns out that the MHD activity drives them to a state in which the chaotic fluctuations are modulated by a low-frequency signal and the oscillators themselves are spatially synchronized. The fact that chaotic oscillators can synchronize their outputs has been intensively investigated both theoretically[26] and experimentally in a wide variety of systems, such as plasma discharge tubes[27] and electronic circuits.[28]

The results presented in Fig. 4 suggest a coupling between electrostatic and magnetic oscillations. We need a better characterization of this phenomenon for a sound conclusion. In particular, we would like to investigate the time evolution of this phase-locking and wave-number condensation due to strong MHD activity. For this task, we shall use other and more powerful numerical tools.

B. Wavelet spectrum analysis

The wavelet spectrum analysis is particularly suited for dealing with data where high time resolution is needed, e.g., for signals with rapidly changing frequencies during short time intervals; hence it is a suitable technique for turbulent data in fluids and plasmas.[29,30] A continuous wavelet transform decomposes the time series using a set of basis functions that changes the size and position by scale factors a and τ, respectively.

Let $x(t)$ be a time series, which can come either from the floating potential $[\tilde{\varphi}(t)]$ or the ion saturation current $[\tilde{n}(t)]$ probes, as well as the Mirnov oscillations $[\tilde{\dot{B}}(t)]$. Its wavelet transform is defined as[31]

$$W_x(a,\tau) = \int x(t)\Psi_a(t-\tau)dt, \tag{1}$$

where the Morlet wavelet is

$$\Psi_a(t) = \frac{1}{\sqrt{2}}\exp\left[i\kappa\frac{2\pi t}{a} - \frac{t^2}{2a^2}\right], \tag{2}$$

such that the frequency and time resolutions are related to the frequency f and scale parameter a according to the value assumed by κ.

The wavelet auto-spectrum of the signal $x(t)$ is

$$S_{xx}(a,T_0) = \int_{T_0-T/2}^{T_0+T/2} W_x(a,\tau)W_x^*(a,\tau)d\tau, \tag{3}$$

and the cross-spectrum between the signals $x(t)$ and $y(t)$ is

$$S_{xy}(a,T_0) = \int_{T_0-T/2}^{T_0+T/2} W_x(a,\tau)W_y^*(a,\tau)d\tau, \tag{4}$$

where T_0 is the center of the time shift interval. The phase angle corresponding to this cross-spectrum is

$$\theta_{xy}(a,T_0) = \tan^{-1}\left\{\frac{\mathrm{Im}[S_{xy}(a,T_0)]}{\mathrm{Re}[S_{xy}(a,T_0)]}\right\}. \tag{5}$$

C. Turbulence modulation by MHD activity

The wavelet spectrogram is a graph showing the normalized value of the auto-spectrum as a function of time. The auto-spectrogram of the Mirnov oscillations, S_{BB}, is shown in Fig. 5(a). It shows, before the application of a DC bias, one major peak at a frequency of approximately 25 kHz and a minor one at ≈13 kHz. After biasing, however, there appear distinct peaks at frequencies that are multiples of a fundamental frequency around f_0=10 kHz. The same peaks (especially the one with the lowest frequency) appear also in the auto-spectrograms of the floating potential [Fig. 5(b)] and the ion saturation current [Fig. 5(c)]. Moreover, it should be mentioned that in the analyzed regime the power spectrum of magnetic fluctuations (S_{BB}) exhibits a slower increase compared to the power spectrum of electrostatic fluctuations ($S_{\varphi\varphi}$ and S_{nn}).

Similar results were also obtained in the other regime, shown in Fig. 3, when the MHD grows without biasing. However, in this case, the rise time of the power spectrum is almost the same for electrostatic and magnetic fluctuations, with the respective maxima being reached almost simultaneously.

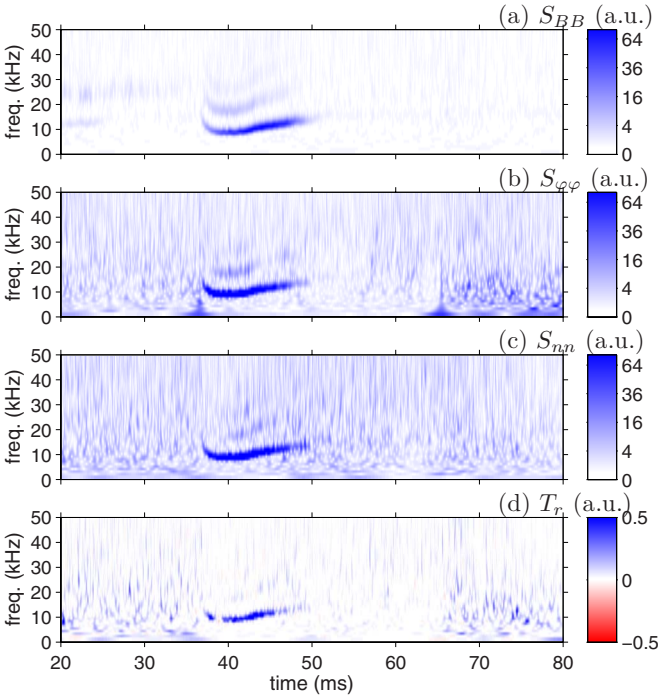

FIG. 5. (Color online) Wavelet spectrogram showing the time evolution of the spectral properties of (a) MHD activity, (b) floating potential, (c) ion saturation current, and (d) transport driven particle flux at r/a=0.94.

In the present analysis, no precursor instability could be identified, such that the enhancement of both strong MHD activity and electrostatic fluctuations seem to take place basically at the same time, and independent of bias.

D. Transport-related fluctuations

The coincident peaks at 10 kHz shown in Fig. 5 indicate the existence of a synchronization of these signals when the MHD activity increases. The synchronization between electrostatic potential and the ion saturation current fluctuations has an important physical consequence, which is the production of a radial particle flux $\Gamma=\langle\tilde{n}\tilde{v}_r\rangle$, where $\tilde{\mathbf{v}}$ is the $\mathbf{E}\times\mathbf{B}$ drift velocity. The fluctuation driven radial particle flux is

$$\Gamma = \frac{\langle\tilde{n}\tilde{E}_\theta\rangle}{B_T}, \tag{6}$$

where B_T is the toroidal equilibrium magnetic field.

The average of the fluctuating density and potential that appears in the above expressions can be readily evaluated through computing the cross-spectrum of both signals, in such a way that the radial particle flux can be written as

$$\Gamma = \int_0^\infty dfT_r(f), \tag{7}$$

where

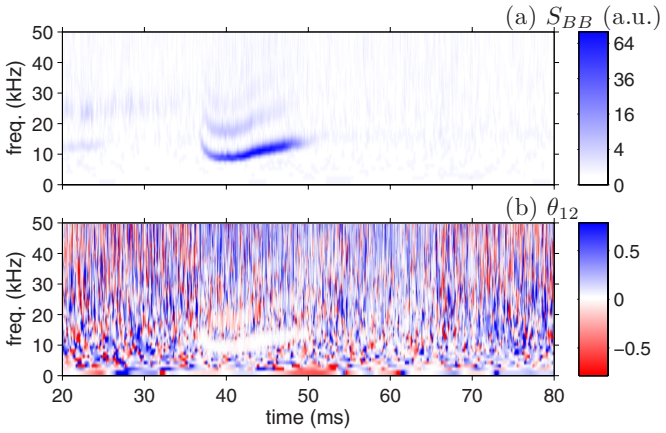

FIG. 6. (Color online) Wavelet spectrogram showing the time evolution of the spectral properties of (a) MHD activity and (b) phase angle between floating potential data sampled at different poloidal locations and $r/a=0.94$.

$$T_r(f) = -\frac{2}{B_T}|S_{\tilde{n}\tilde{E}}(f)|\cos[\theta_{\tilde{n}\tilde{E}}(f)], \tag{8}$$

where $\tilde{E}_\theta \approx -\Delta\varphi/\Delta d$ is the fluctuating poloidal electric field and $\Delta d=0.4$ cm is the distance between probes along the poloidal direction.[32] The wavelet spectral components of the particle flux (7), representing the turbulent driven transport, are depicted in Fig. 5(d). The synchronization with the other signals at the fundamental frequency of $f_0 \approx 10$ kHz is clearly visible.

Our results show that the transport increases in the MHD frequency during the turbulence modulation phase. However, we should mention that biasing the electrode leads to an integrated transport reduction (even during the modulation interval) and an improvement in the confinement quality.[23,24] This can be seen in Fig. 3(b), where there is a moderate density increase after the bias activation at $t=37$ ms. To quantify this reduction, we estimate, from Fig. 5(d), the ratio between the time-averaged turbulent-driven transport at $r/a=0.94$ before and after the biasing as 0.45(5) in the interval without MHD modulation.

E. Phase-locking between potential fluctuations at different poloidal positions

We assumed that the electrostatic potential fluctuations were due to waves propagating in the poloidal direction with phase velocity $v_{ph}=\omega/k$. In addition, Fig. 5 shows that the electrostatic fluctuations are modulated by the MHD activity. This strongly suggests a phase-locking between signals measured at different poloidal positions. We verified this is the case by computing, using Eq. (5), the phase angle θ_{12} related to the cross-spectrum of the potential fluctuations, $\tilde{\varphi}_1(t)$ and $\tilde{\varphi}_2(t)$, measured at different poloidal positions of the plasma column (separated by 0.4 cm). The spectrogram of this phase angle is exhibited in Fig. 6(b), showing a region where this angle is nearly constant and close to zero for the same base frequency f_0 at which the MHD activity is synchronized with the potential fluctuations themselves.

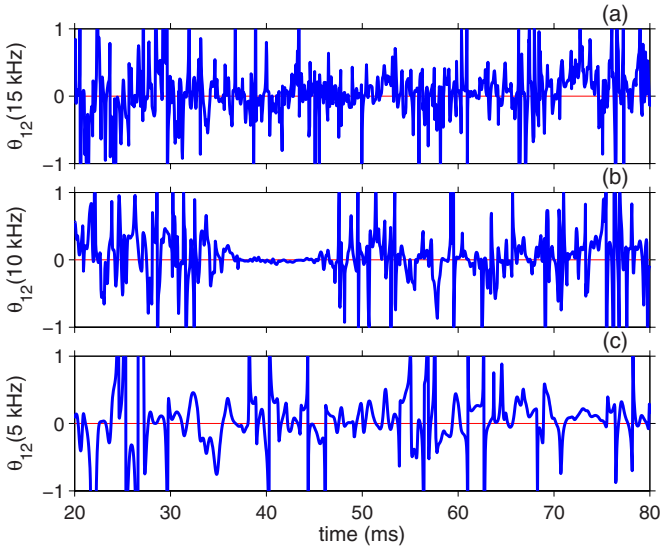

FIG. 7. (Color online) Time evolution of the phase angle between floating potential data sampled at different poloidal locations at (a) $f=15$ kHz, (b) $f=10$ kHz, and (c) $f=5$ kHz.

A further illustration of this synchronization between potential fluctuations at different poloidal position is provided by Fig. 7, where the phase angle itself is plotted against time for three different frequencies, corresponding to horizontal sections made in Fig. 6(b). The synchronization between potential fluctuations at different poloidal positions corresponds to an almost constant phase difference angle near zero at 10 kHz [Fig. 7(b)], a fact not observed for other frequencies [Figs. 7(a) and 7(c)].

F. Phase-locking between potential and ion saturation current fluctuations

Since the electrostatic potential and plasma density evolutions (proportional to ion saturation current fluctuations) are both modulated by the magnetic oscillations, we expect that the potential and density fluctuations are synchronized themselves. However, this and other types of synchronization can also be characterized in a more quantitative way by considering the so-called order parameter, which is a well-known diagnostic of synchronization in problems of nonlinear dynamics.[33]

Let θ_{xy} be the phase angle obtained from the wavelet cross-spectrum of the signals $x(t)$ and $y(t)$. The corresponding order parameter is defined as

$$R_{xy}(t,f) = |\langle e^{i\theta_{xy}}\rangle_t|, \tag{9}$$

which is the magnitude of a centroid phase vector, and the time average

$$\langle e^{i\theta_{xy}}\rangle_t = \frac{1}{\Delta t}\int_{-\Delta t/2}^{\Delta t/2} e^{i\theta_{xy}(\tau+t,f)}d\tau, \tag{10}$$

is computed over an interval of duration $\Delta t=1.5$ ms. A completely synchronized state, like that depicted in Fig. 7(b), is such that the centroid vector is the coherent sum of all phase vectors, thus giving $R_{xy}=1$. Nonsynchronized states, in gen-

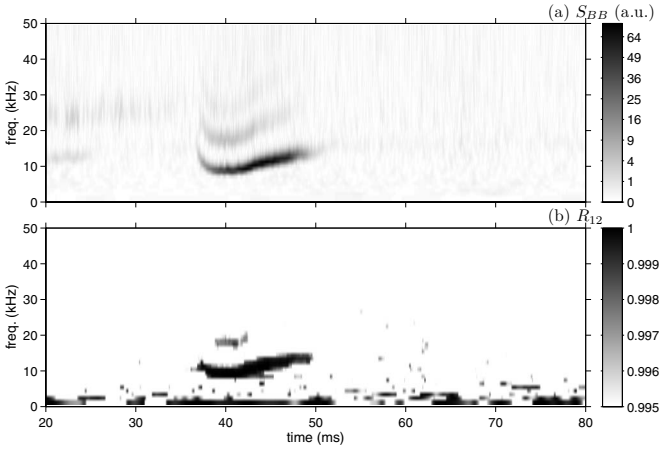

FIG. 8. (a) Wavelet spectrogram of the MHD activity time evolution. (b) Time evolution of the order-parameter magnitude computed for the phase angles between floating potential data sampled at different poloidal locations and $r/a=0.94$.

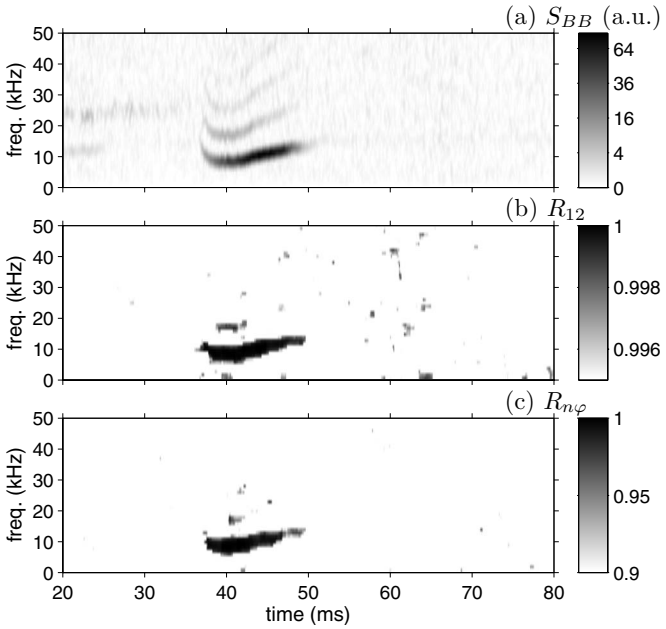

FIG. 9. (a) Windowed Fourier spectrogram of the MHD activity time evolution. (b) Time evolution of the order-parameter magnitude computed for the phase angles between floating potential data sampled at different poloidal locations and $r/a=0.94$. (c) The same as (b), but the phase angle is now computed between floating potential and ion saturation current data at the same poloidal position.

eral, are characterized by lower values of the order parameter.

A wavelet spectrogram of the Mirnov oscillations [Fig. 8(a)] can be compared with that obtained for the order-parameter magnitude $R_{12}(f)$ for the phase angle θ_{12} between floating potentials measured at different poloidal positions [Fig. 8(b)]. A clearly noticeable synchronization band appears in the phase spectrogram, reinforcing our previous claims. However, in the phase spectrogram of Fig. 8(b) some spurious low-frequency bands appear that do not have physical origin, being just numerical artifacts of the wavelet technique due to the fact that the wavelet time resolution in lower frequency is comparable with the interval duration over which the time average in Eq. (10) is computed. One way to circumvent these undesirable results is to use windowed Fourier spectrograms, as illustrated by Fig. 9.

The windowed Fourier spectrograms of the Mirnov fluctuations [Fig. 9(a)] and order-parameter magnitude $R_{12}(f)$ [Fig. 9(b)] are, in fact, similar to their counterparts obtained from wavelet spectra, but the spurious low-frequency bands are now absent. Essentially the same results appear when we plot the wavelet spectrogram of the order-parameter magnitude $R_{\tilde{n}\tilde{\varphi}}(f)$ for the phase angle $\theta_{\tilde{n}\tilde{\varphi}}$ between potential and ion saturation current fluctuations [Fig. 9(c)].

Physical quantities related with electrostatic turbulence typically exhibit a radial dependence, due to the strong density and temperature gradients in the plasma edge region. For example, in a previous work we have analyzed the radial dependence of the degree of deterministic content in time signals of potential fluctuations, and we found that it has a maximum just before the plasma edge.[34] In the present investigation, we observed that the phase-locking and spatial synchronization effects between potential and ion saturation fluctuations and Mirnov oscillations have different intensities dependent on the radial position. We have chosen five radial positions, each of them corresponding to different, albeit similar, plasma discharges.

In order to quantify this radial dependence, we have computed the average order parameters considered here at the time and frequency intervals for which the MHD activity was strong. By "strong activity" we mean an auto-spectral density of the magnetic oscillations, S_{BB}, above a chosen intensity threshold of $\Lambda=10$ a.u. [corresponding to a black part of the magnetic spectrograms, as in Fig. 9(a)]. Our results, summarized in Table I, point out a high level of spatiotemporal coherence for radii between 17.0 and 18.0 cm (plasma edge), decreasing for larger radii (scrape-off layer). In fact, the magnetic surface with $q=3$ is expected to be located near 17.0 cm, and the 3/1 turns to be one of the modes exciting the Mirnov oscillations that drive the electrostatic turbulence in this region.[24]

TABLE I. Radial profiles for the average power spectral and order-parameter values computed for intervals in which the MHD activity is stronger than a threshold $\Lambda=10$. We indicate within parentheses the standard deviation for the order-parameter values measured during MHD activity.

r (cm)	$\langle S_{BB}\rangle_{S_{BB}>\Lambda}$	$\langle R_{12}\rangle_{S_{BB}>\Lambda}$	$\langle R_{n\varphi}\rangle_{S_{BB}>\Lambda}$
17.0	33.8	0.9995(10)	0.98(4)
17.5	32.9	0.9993(8)	0.97(4)
18.0	33.8	0.9986(14)	0.90(10)
19.0	30.8	0.97(3)	0.73(20)
20.0	34.7	0.93(6)	0.45(18)

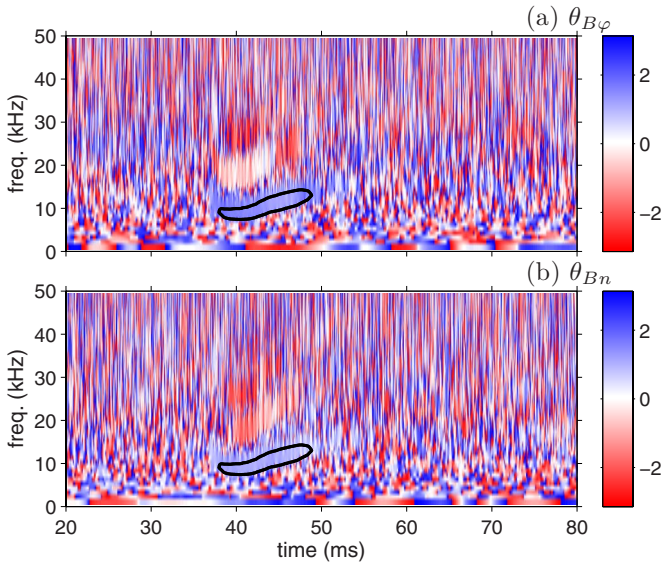

FIG. 10. (Color online) Wavelet spectrogram showing the time evolution of the phase angles between (a) floating potential and MHD activity; (b) plasma density and MHD activity, both considered at $r/a=0.94$.

G. Synchronization between electrostatic and density fluctuations due to MHD activity

We observed that the MHD activity induces a synchronization between electrostatic and density fluctuations. The wavelet spectrograms of the phase angle $\theta_{B\varphi}$ between floating potential fluctuations and MHD activity fluctuations [Fig. 10(a)] and the phase angle θ_{Bn} between plasma density fluctuations and MHD activity fluctuations [Fig. 10(b)] exhibit a common band. The contours of these bands, displayed in Fig. 10, represent level curves indicating that, inside these contours, the MHD activity is strong (in the sense of $S_{BB} \geqslant 10$ a.u., as used in Table I).

The almost constant values of the phase angle in these bands indicate that the fluctuations are synchronized, i.e., although they are not fully correlated in amplitude (even showing different irregular behavior), their phases exhibit coherence, in that their time rates are approximately equal.[26] We emphasize that such an effect has been observed in the presence of MHD activity, the latter being thus interpreted as the physical cause that triggers this effect.

IV. CONCLUSIONS

Correlations between electrostatic and magnetic fluctuations at the turbulent plasma edge region have been detected over recent years in some tokamak experiments, especially when external perturbations enhanced the MHD activity. Such perturbations can be created, for example, by gas puffing, biased electrodes, divertors, and ergodic limiters.

In this paper, we report the observation of an even stronger feature of these correlations, namely the actual synchronization of electrostatic potential fluctuations with those due to MHD activity, measured in the TCABR tokamak. A wavelet spectral analysis revealed that the experimentally observed signals of MHD activity, ion saturation current, and floating potential present spectral peaks at a fundamental frequency of 10 kHz and at least two higher harmonic frequencies. Our results essentially agree with those obtained in the early 1990s in the TEXTUp tokamak (see Ref. 18), and we provide in this work a dynamical characterization for them, in the framework of phase and frequency synchronization.

It is remarkable that, while both MHD activity and turbulent electrostatic fluctuations are present virtually during the entire plasma discharge, these synchronization phenomena were observed only after the MHD activity was enhanced. Since magnetic oscillations already presented discernible frequency peaks (one of them around 13 kHz) before strong MHD activity was increased, we claim that the synchronization occurs because the enlarged MHD activity is actually modulating the electrostatic oscillations. In other words, given that before synchronization the turbulent potential fluctuations present a broadband spectrum, after synchronization their power spectral density is transferred to the characteristic Mirnov frequencies and even some of their harmonics. In TCABR, MHD activity enhancement may appear for two kinds of reproducible discharges. In one of these kinds, this enhancement occurs spontaneously, while in the other kind it appears only after the electrode bias is switched on.

But this synchronization is not restricted to the frequency domain, as we showed by considering potential signals sampled at different poloidal positions in the same discharge, thanks to the use of a two-probe technique. We obtained, through wavelet cross-spectral analysis, a phase angle between such signals that surprisingly presents the same fundamental frequency peak at 10 kHz as the MHD activity does. This is compatible with the poloidal propagation of a long wavelength electrostatic wave of a dominant mode with frequency 10 kHz. Furthermore, we observed that the phase-locking and spatial synchronization effects between potential and ion saturation fluctuations and magnetic oscillations have different intensities according to the radial positions of the probes, with a maximum level at the plasma edge.

In summary, our results provide firm experimental basis to the hypothesis that magnetic and electrostatic fluctuations are not only correlated but also can exhibit phase and frequency synchronization. Such synchronization may be observed in other tokamak discharges with large MHD activity excited by instabilities triggered by the use of control devices like biased electrodes, divertors, and ergodic magnetic limiters.

ACKNOWLEDGMENTS

This work was made possible with partial financial help from FAPESP, CNPq, Fundação Araucária, CAPES, and Rede Nacional de Fusão (RNF-CNEN). I.L.C. and R.L.V. would like to acknowledge Roger D. Bengtson and Phil Morrison for their warm hospitality at the Institute for Fusion Studies, University of Texas at Austin, where this work was completed. The authors also acknowledge useful suggestions and discussions with Murilo Baptista.

[1] A. H. Boozer, Rev. Mod. Phys. **76**, 1071 (2004).
[2] Ch. P. Ritz, R. V. Bravenec, P. M. Schoch, R. D. Bengtson, J. A. Boedo, J. C. Forster, K. W. Gentle, Y. He, R. L. Hickok, Y. J. Kim, H. Lin, P. E. Phillips, T. L. Rhodes, W. L. Rowan, P. M. Valanju, and A. J. Wootton, Phys. Rev. Lett. **62**, 1844 (1989).
[3] W. Horton, Rev. Mod. Phys. **71**, 735 (1999).
[4] C. Hidalgo, C. Alejaldre, A. Alonso, J. Alonso, L. Almoguera, F. de Aragón, E. Ascasíbar, A. Baciero, R. Balbín, E. Blanco, J. Botija, B. Brañas, E. Calderón, A. Cappa, J. A. Carmona, R. Carrasco, F. Castejón, J. R. Cepero, A. A. Chmyga, J. Doncel, N. B. Dreval, S. Eguilior, L. Eliseev, T. Estrada, J. A. Ferreira, A. Fernández, J. M. Fontdecaba, C. Fuentes, A. García, I. García-Cortés, B. Gonalves, J. Guasp, J. Herranz, A. Hidalgo, R. Jiménez, J. A. Jiménez, D. Jiménez-Rey, I. Kirpitchev, S. M. Khrebtov, A. D. Komarov, A. S. Kozachok, L. Krupnik, F. Lapayese, M. Liniers, D. López-Bruna, A. López-Fraguas, J. López-Rázola, A. López-Sánchez, E. de la Luna, G. Marcon, R. Martin, K. J. McCarthy, F. Medina, M. Medrano, A. V. Melnikov, P. Méndez, B. van Milligen, I. S. Nedzelskiy, M. Ochando, O. Orozco, J. L. de Pablos, L. Pacios, I. Pastor, M. A. Pedrosa, A. de la Pea, A. Pereira, A. Petrov, S. Petrov, A. Portas, D. Rapisarda, L. Rodríguez-Rodrigo, E. Rodriguez-Solano, J. Romero, A. Salas, E. Sánchez, J. Sánchez, M. Sánchez, K. Sarksian, C. Silva, S. Schchepetov, N. Skvortsova, F. Tabarés, D. Tafalla, A. Tolkachev, V. Tribaldos, I. Vargas, J. Vega, G. Wolfers, and B. Zurro, Nucl. Fusion **45**, S266 (2005).
[5] G. Li, J. R. Drake, H. Bergsaker, J. H. Brzozowski, G. Hellblom, S. Mazur, A. Möller, and P. Nordlund, Phys. Plasmas **2**, 2615 (1995).
[6] E. D. Frederickson, K. McGuire, A. Cavallo, B. Grek, K. I. Hattori, D. Johnson, and A. W. Morris, Rev. Sci. Instrum. **59**, 1797 (1988).
[7] S. C. McCool, J. Y. Chen, A. J. Wootton, M. E. Austin, R. D. Bengtson, D. L. Brower, W. A. Craven, M. S. Foster, R. L. Hickok, H. Lin, Ch. P. Ritz, P. M. Schoch, B. A. Smith, X. Z. Yang, and C. X. Yu, J. Nucl. Mater. **176-177**, 716 (1990).
[8] S. C. McCool, A. J. Wootton, A. Y. Aydemir, R. D. Bengtson, J. A. Boedo, R. V. Bravenec, D. L. Brower, J. S. DeGrassie, T. E. Evans, S. P. Fan, J. C. Forster, M. S. Foster, K. W. Gentle, Y. X. He, R. L. Hickock, G. L. Jackson, S. K. Kim, M. Kotschenreuther, N. C. Luhmann, Jr., W. H. Miner, Jr., N. Ohyabu, D. M. Patterson, W. A. Peebles, P. E. Phillips, T. L. Rhodes, B. Richards, C. P. Ritz, D. W. Ross, W. L. Rowan, P. M. Schoch, B. A. Smith, J. C. Wiley, X. H. Yu, and S. B. Zheng, Nucl. Fusion **29**, 547 (1989).
[9] T. E. Evans, M. Goniche, A. Grosman, D. Guilhem, W. Hess, and J.-C. Vallet, J. Nucl. Mater. **196-198**, 421 (1992).
[10] Ph. Ghendrih, M. Baucoulet, L. Colas, A. Grosman, R. Guirlet, J. Gunn, T. Loarer, A. Azaroual, V. Basiuk, B. Beaumont, A. Baucoulet, P. Beyer, S. Bramond, J. Bucalossi, H. Capes, Y. Corre, L. Costanzo, C. De Michelis, P. Devynck, S. Faron, C. Friant, X. Garbet, R. Giannella, C. Grisolia, W. Hess, J. Hogan, L. Ladurelle, F. Laugier, G. Martin, M. Mattioli, B. Meslin, P. Monier-Garbet, D. Moulin, F. Nguyen, J.-Y. Pascal, A.-L. Pecquet, B. Pagouria, R. Reichle, F. Saint-Laurent, J.-C. Vallet, M. Zabiago, and the TORE SUPRA Team, Nucl. Fusion **42**, 1221 (2002).
[11] Y. Xu, R. R. Weynants, S. Jachmich, M. Van Schoor, M. Vergote, P. Peleman, M. W. Jakubowski, M. Mitri, D. Reiser, B. Unterberg, and K. H. Finken, Phys. Rev. Lett. **97**, 165003 (2006).
[12] V. Budaev, Y. Kikuchi, Y. Uesugi, and S. Takamura, Nucl. Fusion **44**, S108 (2004).
[13] T. E. Evans, R. A. Moyer, K. H. Burrell, M. E. Fenstermacher, I. Joseph, A. W. Leonard, T. H. Osborne, G. D. Porter, M. J. Schaffer, P. B. Snyder, P. R. Thomas, J. G. Watkins, and W. P. West, Nat. Phys. **2**, 419 (2006).
[14] S. J. Camargo, B. D. Scott, and D. Biskamp, Phys. Plasmas **3**, 3912 (1996)
[15] A. Hasegawa and M. Wakatani, Phys. Rev. Lett. **50**, 682 (1985).
[16] P. Beyer, X. Garbet, S. Benkadda, P. Ghendrih, and Y. Sarazin, Plasma Phys. Controlled Fusion **44**, 2167 (2002).
[17] C. Schröder, T. Klinger, D. Block, A. Piel, G. Bonhomme, and V. Naulin, Phys. Rev. Lett. **86**, 5711 (2001); T. Klinger, C. Schröder, D. Block, F. Greiner, A. Piel, G. Bonhomme, and V. Naulin, Phys. Plasmas **8**, 1961 (2001).
[18] H. Lin, Ph.D. thesis, University of Texas, Austin (1991).
[19] M. V. A. P. Heller, R. M. Castro, Z. A. Brasílio, I. L. Caldas, and R. P. Silva, Nucl. Fusion **35**, 59 (1995).
[20] P. Devynck, J. Stöckel, J. Adamek, I. Duran, M. Hron, and G. Van Oost, Czech. J. Phys. **53**, 853 (2003).
[21] P. Devynck, G. Bonhomme, E. Martines, J. Stöckel, G. Van Oost, I. Voitsekhovitch, J. Adámek, A. Azeroual, F. Doveil, I. Duran, E. Gravier, J. Gunn, and M. Hron, Plasma Phys. Controlled Fusion **47**, 269 (2005).
[22] M. V. A. P. Heller, I. L. Caldas, A. A. Ferreira, E. A. O. Saettone, and A. Vannucci, J. Plasma Phys. **73**, 295 (2007).
[23] I. C. Nascimento, Yu. K. Kuznetsov, J. H. F. Severo, A. M. M. Fonseca, A. Elfimov, V. Bellintani, M. Machida, M. V. A. P. Heller, R. M. O. Galvão, E. K. Sanada, and J. I. Elizondo, Nucl. Fusion **45**, 796 (2005).
[24] I. C. Nascimento, Yu. K. Kuznetsov, Z. O. Guimarães-Filho, I. El Chamaa-Neto, O. Usuriaga, A. M. M. Fonseca, R. M. O. Galvão, I. L. Caldas, J. H. F. Severo, I. B. Semenov, C. Ribeiro, M. V. P. Heller, V. Bellintani, J. I. Elizondo, and E. Sanada, Nucl. Fusion **47**, 1570 (2007).
[25] R. M. O. Galvão, Y. K. Kuznetsov, I. C. Nascimento, E. Sanada, D. O. Campos, A. G. Elfimov, J. I. Elizondo, A. N. Fagundes, A. A. Ferreira, A. M. M. Fonseca, E. A. Lerche, R. Lopez, L. F. Ruchko, W. P. de Sá, E. A. Saettone, J. H. F. Severo, R. P. da Silva, V. S. Tsypin, R. Valencia, and A. Vannucci, Plasma Phys. Controlled Fusion **43**, 1181 (2001).
[26] A. S. Pikovsky, M. G. Rosenblum, and J. Kurths, *Synchronization: A Universal Concept in Nonlinear Sciences* (Cambridge University Press, Cambridge, 2003); *Synchronization: Theory and Application*, edited by A. S. Pikovsky and Y. Maistrenko (Kluwer, Dordrecht, 2003).
[27] C. M. Ticos, E. Rosa, Jr., W. B. Pardo, J. A. Walkenstein, and M. Monte, Phys. Rev. Lett. **85**, 2929 (2000).
[28] M. S. Baptista, T. Pereira, J. C. Sartorelli, I. L. Caldas, and J. Kurths, Physica D **212**, 216 (2005).
[29] M. Farge, Annu. Rev. Fluid Mech. **24**, 395 (1992).
[30] J. E. Ruppert-Felsot, O. Praud, E. Sharon, and H. L. Swinney, Phys. Rev. E **72**, 016311 (2005).
[31] B. Ph. van Milligen, C. Hidalgo, E. Sánchez, M. A. Pedrosa, R. Balbín, I. García-Cortés, and G. R. Tynan, Rev. Sci. Instrum. **68**, 967 (1997).
[32] Ch. P. Ritz, E. J. Powers, and R. D. Bengtson, Phys. Fluids B **1**, 513 (1989).
[33] S. E. de S. Pinto and R. L. Viana, Phys. Rev. E **61**, 5154 (2000).
[34] Z. O. Guimarães-Filho, I. L. Caldas, R. L. Viana, J. Kurths, I. C. Nascimento, and Y. K. Kuznetsov, Phys. Lett. A **372**, 1088 (2008).